PAPER
Robust Design Method of Multilayer Antireflection Coating for Organic Solar Cells

Shigeru KUBOTA[†a], *Member*, Kensaku KANOMATA[†], Katsuaki MOMIYAMA[†],
Takahiko SUZUKI[†], *Nonmembers*, *and* Fumihiko HIROSE[†], *Member*

SUMMARY   We present an optimization algorithm for the design of multilayer antireflection (AR) coatings for organic photovoltaic (OPV) cells. When a set of available materials for the AR films is given, the proposed method allows for searching the globally optimized AR structure that maximizes the short-circuit current density (J_{SC}) under simulated solar light illumination (AM 1.5). By applying this method to an OPV solar cell with a configuration of Al/P3HT:PCBM/MoO$_3$/ITO, we demonstrated that J_{SC} can increase by 7.5% with a 6-layer AR coating, consisting of MgF$_2$, ZnS, and Al$_2$O$_3$. A notable feature of this method is that it can find not only the optimal solution, which maximizes J_{SC}, but also the quasi-optimal solutions, which increase J_{SC} to nearly maximum levels. We showed that the quasi-optimal solution may have higher robustness against deviations in film thicknesses, from their designated values. This method indicates the importance of practically useful, non-optimal solutions for designing AR coatings. The present method allows for extending the user's choices and facilitates the realization of a practical design for an AR coating.

key words: organic solar cell, multilayer antireflection coating, optimization, optical simulation

1. Introduction

Organic photovoltaics (OPVs) have been attracting considerable attention owing to their notable properties such as flexibility, light weight, and low material cost [1], [2]. In the past decade, the power conversion efficiency (PCE) of OPVs has drastically increased to 10% [3]. Many works have been devoted to developing materials for better solar energy harvesting [4], [5] and to establishing methods for efficient large-scale production [6], [7].

An important factor limiting the efficiency of OPVs is the low carrier mobility of organic semiconductors [8]–[10]. Although the photo absorption of organic semiconductors is generally high, efficient extraction of charge carriers from them is difficult. Therefore, the thickness of the active layer needs to be restricted to as low as 100 nm to achieve efficient carrier extraction [10], [11]. To maximize light absorption in the thin active layer, new methods have been developed for light trapping using nanostructures [10], [12] and optical spacers [13] (for a review, see [9]).

Here, we examine an alternative approach to light trapping for OPVs. We examine the multilayer AR films that are deposited on both sides of the glass substrate, to maximize short-circuit current density (J_{SC}). The problem of global optimization of multilayer AR structures for solar cells is a topic of ongoing research [14]–[16]. This problem is difficult to solve because of the high cost of evaluating the objective function and the existence of many local optimal solutions [16]. The structure of multilayer AR films suited for solar cells with thin absorbers has not yet been fully understood [14]. We propose a robust optimization method that can evaluate the level of the decrease in performance due to deviations in film thicknesses from optimized values. It is quite important to consider the effects of such deviations, since low-cost commercial techniques used to deposit AR films necessarily produce variations in film thicknesses [17].

The proposed method optimizes the layer configuration of the AR film when a set of available materials are given in advance. This method can search not only the optimal solution that maximizes J_{SC} but also quasi-optimal solutions that correspond to nearly maximum values of J_{SC}. We showed that the quasi-optimal solutions could be more robust against the variations in film thicknesses and simpler than the optimal solution. Furthermore, in comparison to the proposed method, we examined multilayer AR coatings (ARCs) designed by optimizing the refractive index for each layer as in the case of materials with a controlled porosity [18], [19]. Additionally, we compared performances between the AR films deposited on the front and back sides of the substrate. These results provide insights for realizing a robust and simple ARC design for practical application to OPVs.

2. Methods

2.1 Proposed Optimization Algorithm

We propose an optimization algorithm to design multilayer AR films for OPVs. The objective of this algorithm is to determine the material and thickness for each AR layer to achieve the highest J_{SC}, given a set of available materials. A P3HT:PCBM-based OPV shown in Fig. 1 (left) was used as a typical example in this study. In this example, the OPV device contains a total of 6 layers of ARC on both sides of the substrate (3 layers on each side).

The block diagram of the proposed algorithm is presented in Fig. 2. As shown in this diagram, the algorithm is characterized by a double loop. In the outer loop (Steps (1–6) in Fig. 2), all possible combinations of materials are examined, while in the inner loop (Steps (2–4) in Fig. 2),

the optimization of the film thicknesses is executed for each material combination. To obtain the global optimal solution efficiently in the inner loop, we used the multistart algorithm [20]. In this 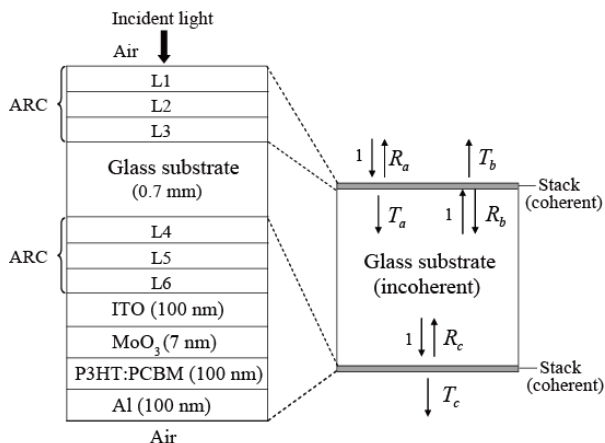algorithm, local searches, such as the quasi-Newton method, are performed from random initial points. In Step (4) in Fig. 2, the number of cycles of local searches (N) is set to 50. Increasing this number to 75 or 100 did not change the optimal solution in our example (Fig. 1). The effects of deviations in film thicknesses from their designated values are evaluated in Step (7) in Fig. 2. Here, the decrease in J_{SC} by such deviations is estimated as δJ_{SC} (see below). Rows 1–4 in Table 1 show an example of the solution list generated in Step (7) in Fig. 2. The solution list contains the increase rate in J_{SC} due to the ARC for each solution in the absence and presence of deviations in the film thicknesses (γ and $\tilde{\gamma}$, respectively; see below).

If a 6-layer ARC (as in Fig. 1 (left)) is designed with 3 different materials, there exist 144 possible combinations of materials excluding cases where the same material is used for adjacent layers. Therefore, the cycle number of the quasi-Newton method becomes 7,200 (= 144 × 50). This corresponds to a computation time of around 1 h using an Intel Core i7 personal computer (2.93 GHz) and program code written in C++.

For comparison to the proposed algorithm, we performed global optimization of the refractive indexes and thicknesses of AR layers without making assumptions about specific materials (the bottom row in Table 1). The multistart algorithm [20] was used for the optimization algorithm.

Fig. 1 Examined structure of OPV. The left figure represents the material and layer thickness (in parentheses) for each layer. The six layers, labeled as L1–L6, show the AR films to be designed. As illustrated in the right figure, the OPV consists of two thin film stacks and a glass substrate that is much thicker than the stacks.
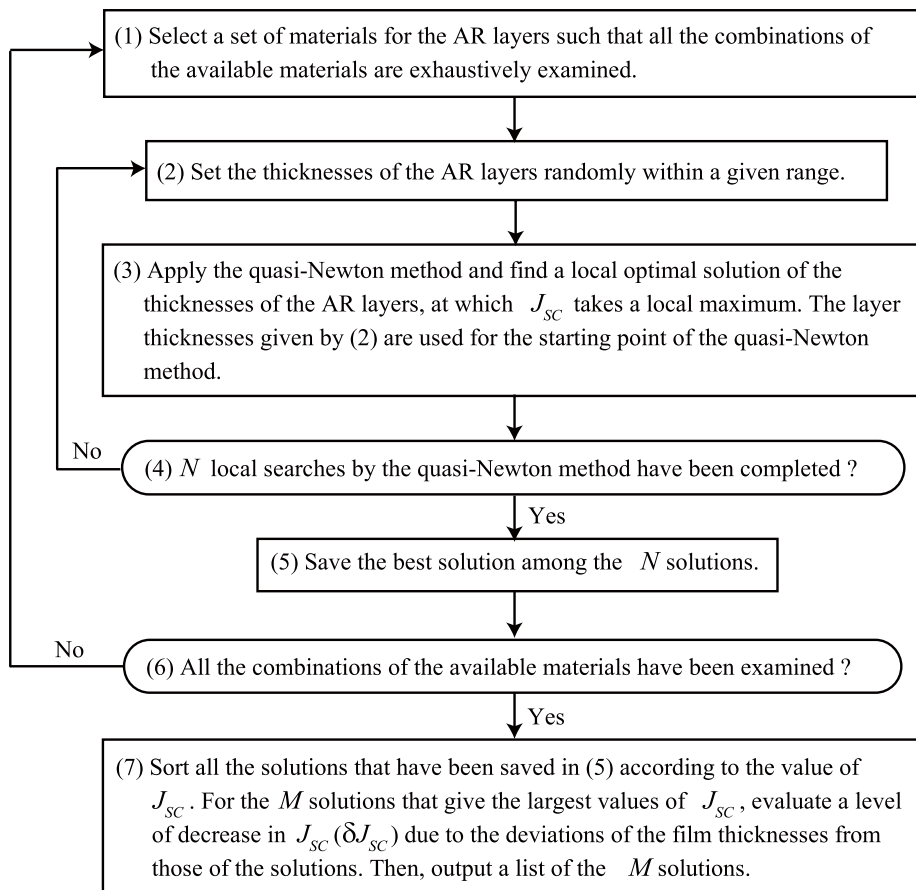

Fig. 2 Proposed optimization algorithm.

Table 1   A list of the configuration of ARCs obtained by the optimization.

No.	L1	L2	L3	L4	L5	L6	$\gamma / \tilde{\gamma}$ (%)
1	MgF_2 (92)	ZnS (6)	Al_2O_3 (104)	MgF_2 (144)	Al_2O_3 (135)	MgF_2 (35)	7.51/6.97
2	MgF_2 (81)	Al_2O_3 (120)	–	MgF_2 (144)	Al_2O_3 (135)	MgF_2 (35)	7.39/7.17
3	MgF_2 (93)	ZnS (7)	Al_2O_3(101)	Al_2O_3 (195)	ZnS (104)	MgF_2 (31)	7.26/6.59
4	MgF_2 (75)	Al_2O_3 (112)	MgF_2 (172)	MgF_2 (162)	ZnS (106)	MgF_2 (33)	7.18/6.60
–	n=1.19 (102)	n=1.44 (254)	–	n=1.08 (212)	n=2.07 (124)	n=1.05 (30)	10.39/9.72

All rows other than the bottom one (i.e., No. 1–4) show the solutions of ARCs obtained by the proposed optimization method using the materials of MgF_2, ZnS, and Al_2O_3. The entries for solution No. 1–4 represent the materials and thicknesses (values in parentheses) for layers L1–L6 in Fig. 1. The rightmost entries show the increase in J_{SC} in the absence and presence of deviations in layer thicknesses from their design values (γ and $\tilde{\gamma}$, respectively). Solution No. i ($i = 1, \dots, 4$) corresponds to the ARC that produces the i th largest value of J_{SC} in the absence of deviations in layer thicknesses. The bottom row shows the ARC with optimized refractive indexes and layer thicknesses (the values of n and those in parentheses, respectively). The '–' marks in L3 mean that the thickness of this layer converges to 0 as a result of optimization.

The refractive index of each AR layer is supposed to assume an arbitrary value between 1.05 and 2.7, which corresponds to materials with controlled porosity [21].

2.2 Estimating the Effects of Deviations in Film Thicknesses on J_{SC}

The effects of deviations in the thicknesses of AR films on J_{SC} were examined in our algorithm (Step (7) in Fig. 2). We define δJ_{SC} to be the expected decrease in J_{SC} when the thicknesses of all the AR layers exhibit independent deviations from those of the (local) optimal solutions. Then, δJ_{SC} is described by the following equation:

$$\delta J_{SC} = \frac{1}{2^p} \sum_{i=1}^{2^p} \left[J_{SC}(\mathbf{d}^*) - J_{SC}(\mathbf{d}^* + \Delta \mathbf{d}^i) \right]. \tag{1}$$

Here, $\mathbf{d}^*$ denotes the vector composed of the thicknesses of AR layers corresponding to the solution, where the size of the vector p is the same as the number of AR layers. The term $\Delta \mathbf{d}^i$ ($i = 1, \dots, 2^p$) is the vector having size p to determine the magnitude and direction of the deviations in the film thicknesses. Throughout this study, the deviation in the thickness of each AR layer is set to be ± 5 nm. Thus, in the case of $p = 2$, for example, we have $\Delta \mathbf{d}^1 = (5 \text{ nm}, 5 \text{ nm})$, $\Delta \mathbf{d}^2 = (5 \text{ nm}, -5 \text{ nm})$, $\Delta \mathbf{d}^3 = (-5 \text{ nm}, 5 \text{ nm})$, and $\Delta \mathbf{d}^4 = (-5 \text{ nm}, -5 \text{ nm})$. Generally, the vectors of $\Delta \mathbf{d}^i$ ($i = 1, \dots, 2^p$) lie on the vertices of a p-dimensional hypercube with the length of each side equal to 10 nm with the center at the origin. $J_{SC}(\mathbf{d})$ denotes the value of J_{SC} corresponding to an AR film whose layer thicknesses are represented by the p-dimensional vector $\mathbf{d}$. Therefore, $J_{SC}^* \equiv J_{SC}(\mathbf{d}^*)$ corresponds to J_{SC} for the solution corresponding to the vector $\mathbf{d}^*$. We introduce $\tilde{J}_{SC} \equiv J_{SC}^* - \delta J_{SC} = \frac{1}{2^p} \sum_{i=1}^{2^p} J_{SC}(\mathbf{d}^* + \Delta \mathbf{d}^i)$ to be the short-circuit current density that can be expected to be obtained with deviations in the AR film thicknesses. By defining J_{SC}^0 as J_{SC} without the AR coatings (i.e., the original J_{SC} value of the solar cell), we use $\gamma = J_{SC}^*/J_{SC}^0 - 1$ and $\tilde{\gamma} = \tilde{J}_{SC}/J_{SC}^0 - 1$ as the standard by which to evaluate AR performance, for the cases without and with deviations in the film thickness, respectively.

Note that in our algorithm (Fig. 2), δJ_{SC} is evaluated solely for the solutions that have been saved in (5). Obvi-

ously, it is possible to incorporate the effects of deviations in the film thicknesses into the objective function used for the local searches (Step (3) in Fig. 2). However, the evaluation of the effects of such deviations requires a high computational effort since this should generally be accompanied by a procedure for changing the thicknesses of all AR layers independently and calculating J_{SC}. It would be practically sufficient to evaluate the effects of deviations solely for the local optimal solutions, as in our algorithm. This is because in the neighborhood of these solutions, J_{SC} does not change with respect to the first-order variations in the layer thicknesses, and thus they are intrinsically quite robust against deviations.

2.3 Optical Analysis by Characteristic Matrix Method

We performed optical analysis of OPVs using the characteristic matrix method [22]. As shown in Fig. 1, the solar cell structure with an ARC, which was considered in this study, contains two thin film stacks and a much thicker glass substrate. Therefore, as in previous studies [23], [24], we assumed that internally within the thin multilayer stacks, the light is added coherently by the characteristic matrix-based formalism, whereas for the thick substrate, the coherence is lost, and the addition of irradiances (not optical field amplitudes) is considered. The procedures for calculating J_{SC} are summarized as follows.

The reflectance R and transmittance T for a multilayer stack (with q layers) are generally described by the following equations [22]:

$$R = \left(\frac{\eta_i B - C}{\eta_i B + C} \right) \left(\frac{\eta_i B - C}{\eta_i B + C} \right)^*, \tag{2}$$

and

$$T = \frac{\text{Re}(\eta_e)}{\text{Re}(\eta_i)} \left(\frac{2\eta_i}{\eta_i B + C} \right) \left(\frac{2\eta_i}{\eta_i B + C} \right)^*, \tag{3}$$

where η_i and η_e are the optical admittances of the incident and emergent media, respectively. Here, B and C are obtained as

$$\begin{bmatrix} B \\ C \end{bmatrix} = M_1 M_2 \cdots M_q \begin{bmatrix} 1 \\ \eta_e \end{bmatrix}, \tag{4}$$

where the characteristic matrix M_r for the rth layer is

$$M_r = \begin{bmatrix} \cos \delta_r & (i \sin \delta_r)/\eta_r \\ i\eta_r \sin \delta_r & \cos \delta_r \end{bmatrix}. \tag{5}$$

In this matrix, δ_r denotes the phase difference between the top and bottom of the rth layer, and η_r is the optical admittance for the rth layer.

We assume the active layer (i.e., P3HT:PCBM) to be the pth layer in a multilayer stack, and denote the absorbance in the active layer as A_p. Then, we can find

$$A_p = I_s(\psi_{p-1} - \psi_p), \tag{6}$$

$$\psi_r = \frac{\mathrm{Re}(B_r C_r^*)}{\mathrm{Re}(BC^*)} \quad \text{(for all } r\text{)}, \tag{7}$$

$$\begin{bmatrix} B_r \\ C_r \end{bmatrix} = M_{r+1} M_{r+2} \cdots M_q \begin{bmatrix} 1 \\ \eta_e \end{bmatrix}, \tag{8}$$

where ψ_p is the potential transmittance [22], [24] for the subassembly, including the structure from the incident surface to the pth layer, within the stack containing the active layer. I_s is the irradiance entering this stack. By taking into consideration the multiple reflection at the interfaces between the substrate and both the stacks (Fig. 1, right), I_s can be described as

$$I_s = \frac{T_a T_c}{\psi_t(1 - R_b R_c)}, \tag{9}$$

where R_b, R_c, T_a, and T_c are the reflectance and transmittance defined as shown in Fig. 1 (right). ψ_t is the potential transmittance of a whole multilayer stack containing the active layer.

We denote the absorbance in the active layer at wavelength λ as $A_p(\lambda)$. Then, the number of photons absorbed in the active layer, corresponding to wavelength λ, becomes

$$N_p(\lambda) = A_p(\lambda)F(\lambda)\frac{\lambda}{hc}. \tag{10}$$

Here, $F(\lambda)$ represents the spectrum of solar irradiance given by the AM 1.5 standard [25], h is the Planck constant, and c is the speed of light in vacuum.

Using the unit charge q, we can convert the number of photons into the generated photocurrent as follows:

$$J_{SC} = \int_0^{\lambda_g} qN_p(\lambda)F_{NR}(\lambda)d\lambda, \tag{11}$$

where λ_g is the wavelength corresponding to the band gap energy of P3HT (653 nm), and $F_{NR}(\lambda)$ is the non-recombination factor, which for simplicity we assume to be 1 at all λ [26].

We also investigated the depth profile of light absorbance within solar cells. We define $\psi(z)$ to be the potential transmittance for the substructure from the incident surface to a point within a multilayer stack, which is separated from the surface by distance z [22], [24]. Then, the spatial distribution of the absorbed energy is described as $(1 - R)\psi'(z)$. We obtained this value with changing z and wavelength λ to plot Fig. 3(c).

For the range of wavelengths of interest (300–700 nm) the optical data were taken from the following studies: Hoppe et al. [27] for Glass and ITO, Szekeres et al. [28] for MoO$_3$, Lioudakis et al. [29] for P3HT:PCBM (with the 50:50 wt%), Gray [30] for Al, Borgogno et al. [31] for MgF$_2$, Flory et al. [32] for ZnS, and Palik [33] for Al$_2$O$_3$.

3. Experimental Results

To examine the applicability of the proposed optimization algorithm, we applied it to design the 6-layer AR films shown in Fig. 1 (left). The materials for ARC were selected from MgF$_2$, ZnS, and Al$_2$O$_3$, all of which are typically used for AR films (e.g., [34]). The configuration of the optimized AR layers is shown in solution No. 1 (top row) in Table 1, showing that the ARC enhances J_{SC} by 7.51% and 6.97% in the absence and presence, respectively, of deviations in the film thicknesses from their design values. To elucidate the optical properties of the ARC, in Fig. 3(a), we plotted the absorption spectra of P3HT:PCBM in the OPV for the cases with and without the ARC (red and black lines, respectively). The figure shows that the ARC enhances the photo absorption in P3HT:PCBM in a wide wavelength range, mainly from 450 nm to 650 nm. The green line in Fig. 3(a) shows, for comparison, the absorption spectrum for the case of incorporating AR films whose refractive indexes and layer thicknesses are optimized (see Methods). As shown in the bottom row of Table 1, applying the AR films with the optimized refractive indexes can increase J_{SC} by 10.39%, which is higher than the case only with the available materials (7.51%), as expected, due to increased freedom in designing the ARC configuration.

The depth profiles of absorbance in Fig. 3(b) indicate that the absorbance in P3HT:PCBM is quite high (~ 0.8) at relatively shorter wavelengths of 450 nm and less, except for very short wavelengths of less than 330 nm where the irradiance of the simulated sunlight remains very weak (Fig. 3(a), blue line). However, as the wavelength increases, the light absorption tends to gradually decrease. In particular, in the wavelength range near the band gap of P3HT ($\lambda = 653$ nm), a strong increase in both the reflectance at the solar cell surface and the absorption in Al leads to the decrease of absorption considerably in the active layer (Figs. 3(b) and 3(c)).

As shown in Fig. 4(a), as the wavelength increases, the refractive index of P3HT:PCBM increases considerably to more than 2.5 while its extinction coefficient decreases to near 0. It is likely that for longer wavelengths, these changes in the optical constants may serve to increase the reflectance and to decrease the absorbance in P3HT:PCBM (Fig. 3(b)). However, it is not clear how the strong absorption takes place in Al at longer wavelength (Figs. 3(b) and 3(c)). To clarify this, we examined how the transmittance from P3HT:PCBM into Al depends on their optical parameters. If we define n_0 and k_0 to be, respectively, the refractive index and extinction coefficient of the incident medium (i.e., P3HT:PCBM), and n_1 and k_1 to be those of the emergent medium (i.e., Al), then the transmittance T between the 2
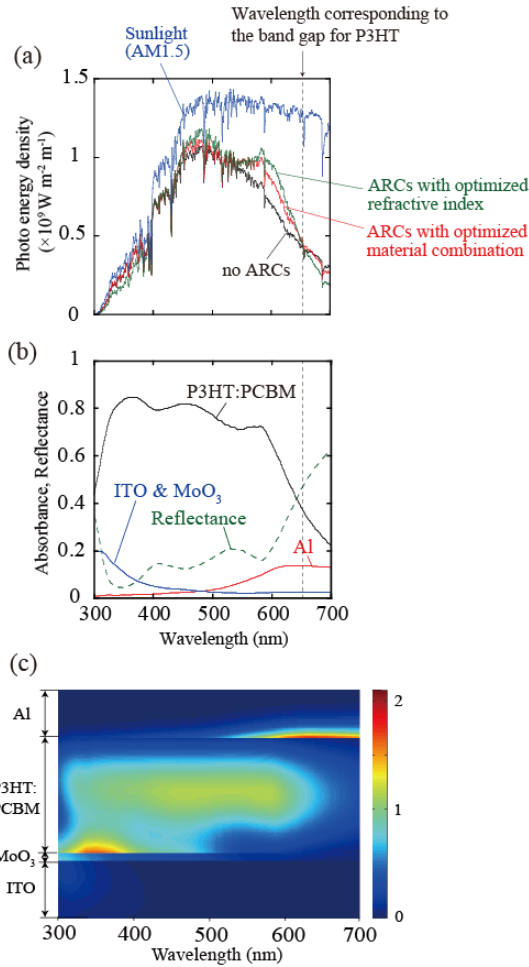
Fig. 3 Spectral properties of an OPV. (a) The spectrum of absorption energy in P3HT:PCBM is plotted in the absence (black) and presence (red and green) of ARCs. The red line shows the case of using the ARC obtained by the proposed method, which optimizes the material combination and layer thicknesses. The green line represents the case of using the ARC obtained by optimizing the refractive indexes and layer thicknesses. The blue line shows the spectrum of sunlight energy given by the AM 1.5 standard. (b) The absorbance in P3HT:PCBM (black), Al (red), ITO and MoO_3 (blue), as well as the reflectance (green) are shown as function of the wavelength, for the OPV with the ARC optimized by the proposed method. (c) The spatial and spectral distribution of absorption in the OPV with the same ARC as in (b).

media can be described as

$$T = \frac{4(n_1/n_0)(n_0^2 + k_0^2)}{(n_0 + n_1)^2 + (k_0 + k_1)^2}. \tag{12}$$

In Fig. 4(c), we plotted changes in T as function of wavelength by using the values of n_0, k_0, n_1, and k_1 shown in Figs. 4(a) and 4(b). The result clearly indicates that the transmittance from P3HT to Al considerably increases with increasing wavelength, which can explain the occurrence of strong absorbance in Al (Figs. 3(b) and 3(c)).

A notable advantage of our design method is that it can find not only the optimal solution (No. 1 in Table 1) but also the quasi-optimal solutions (No. 2–4 in Table 1), which give the values of J_{SC} near the optimized value. For each solu-
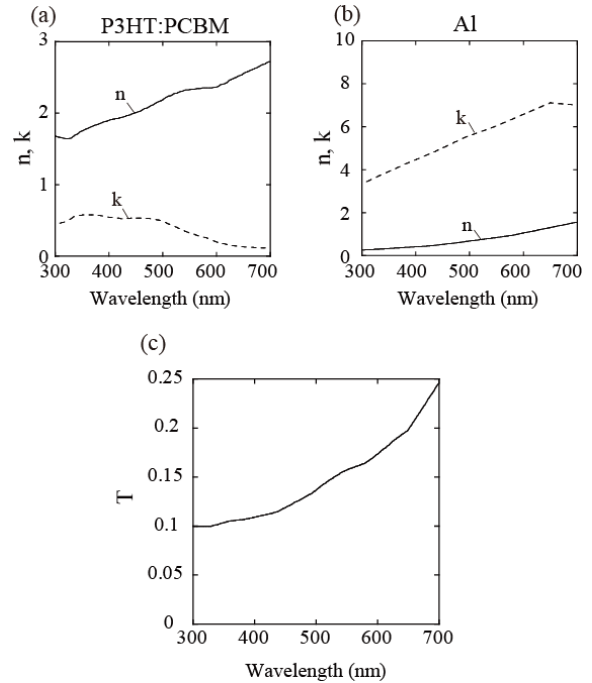

Fig. 4 (a) and (b) Optical properties of P3HT:PCBM (a) and Al (b) [29, 30]. The solid and dashed lines show the refractive index (n) and the extinction coefficient (k), respectively, as function of wavelength. (c) Changes in transmittance T (Eq. 12) from P3HT:PCBM to Al obtained using the optical parameters in (a) and (b).

tion, our algorithm calculates the enhancement in J_{SC} due to applying ARCs in the absence and presence of deviations in film thicknesses from the designated values (γ and $\tilde{\gamma}$, respectively, in Table 1). As seen in Table 1, without deviations, the value of J_{SC} for solution No. 2 is slightly lower than that for solution No. 1 by about 0.1% ($\gamma = 7.51\%$ (No. 1) and 7.39% (No. 2)). Importantly, however, with deviations the order relationship can be reversed such that the J_{SC} value for solution No. 2 becomes higher than that of solution No. 1 by 0.2% ($\tilde{\gamma} = 6.97\%$ (No. 1) and 7.17% (No. 2)). Therefore, by selecting the quasi-optimal solution instead of the optimal solution, we can select a more robust solution in the presence of variations in film thicknesses. This may allow for a more stable result in mass production. Furthermore, the solution No. 1 in Table 1 requires all 6 layers and 3 materials (MgF_2, ZnS, and Al_2O_3) that are available for designing, whereas solution No. 2 consists of 5 layers and 2 different materials (MgF_2, and Al_2O_3) only. This implies that production of the ARC in solution No. 2 would be simpler than the ARC in solution No. 1, indicating further the benefit of making comparisons among the near-optimal solutions.

Additionally, we compared the ARCs on the front, back, and both sides of the substrate (Fig. 5). The white bars in Fig. 5 show the increase in J_{SC} by the 6-layer ARC (i.e., solution No. 1 in Table **1**) and by the 3-layer ARC on either the front or back side of the substrate (L1–L3 or L4–L6 in Fig. 1 (left), respectively). Here, these ARCs were obtained by the proposed optimization method. For comparison, in the gray bars in Fig. 5, we show the changes in J_{SC} by
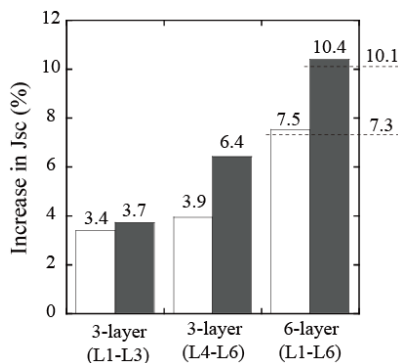
Fig. 5 ARCs on the front and/or back sides of the substrate. The lengths of the bars show the increase in J_{SC} by the 3-layer ARC on either the front or back side of the substrate (L1–L3 or L4–L6, respectively, in Fig. 1) and that by the 6-layer ARC (L1–L6 in Fig. 1), as described below the bars. White bars: the cases of applying the ARCs obtained by the proposed method that optimizes the material combination and layer thicknesses. Gray bars: the cases of applying the ARCs obtained by optimizing the refractive indexes and layer thicknesses. The horizontal dashed lines show the increase in J_{SC} obtained by simply adding the effects of the two 3-layer ARCs for both optimization methods.

the 3-layer and 6-layer ARCs similarly, except for using the AR films designed by optimizing the refractive indexes and layer thicknesses (see Methods). The results indicate that the AR films on the back side of the substrate are more effective than those on the front side, and that this difference is significantly greater for the AR film with the refractive index optimized. Table 1 (bottom row) suggests that the material with very low refractive index is optimal for L4 and L6 (n = 1.08 and 1.05, respectively), which may underlie the fact that the availability of an arbitrarily controlled refractive index is particularly beneficial for L4–L6. The increase rate in J_{SC} by the 6-layer ARC is nearly equal to a simple summation of the effects of the two 3-layer ARCs for the both types of optimization methods (Fig. 5, dashed horizontal lines).

4. Conclusions

In this study, we proposed a method to design the multilayer ARCs for OPVs. This method can globally optimize the materials and thicknesses of AR films, when a set of available materials is given. By applying 6-layer ARC, consisting of the materials selected from MgF_2, ZnS, and Al_2O_3, we have obtained an increase rate in J_{SC} by 7.51% (No. 1 in Table 1) with the AM1.5 solar spectrum at normal incidence. For comparison, we additionally examined the optimization of refractive indexes and layer thicknesses of ARCs, showing an improvement in the performance by 10.39% (the bottom row in Table 1). These results are comparable to the outcome of a recent study examining nanostructured ARCs for OPVs, which has demonstrated 9.4% relative improvement (from 12.6 to 13.8 m A/cm^2) in J_{SC} [12].

A main difficulty in optimizing multilayer ARCs lies in the existence of a number of local optimal solutions, as mentioned above [14]. Therefore, to overcome this problem, global optimization techniques, such as genetic algo-

rithm [16], [18], simulated annealing [36], and a method similar to ours combining random and local searches [14], have been proposed. A novel feature of our method is that it can find not only the optimal solution but also quasi-optimal solutions and construct a list of solutions (Table 1) to make the comparison among them easier. This idea is quite simple but practically important because the quasi-optimal solutions may be more robust against manufacturing errors and simpler in the layer configuration than the optimal solution, and thereby have a greater potential advantage in the application (as in solution No. 2 in Table 1). The present study would be the first to demonstrate the importance of actively seeking "valuable non-optimal" solutions in designing ARCs. In the future work, it would be important to extend the proposed optimization method to include the effect of variations in angles of incident (AOI) [15], [35], and develop multilayer ARCs that are robust against the variations in both layer thicknesses and AOI.

In addition, we examined the wavelength-dependent properties of light absorption in the OPVs (Fig. 3). An important finding was that the combination of optical constants of P3HT:PCBM and Al at longer wavelengths produces strong absorbance in Al (Fig. 4). It would be important to examine a method to prevent absorption in the metal and to strengthen the backside reflection. Furthermore, we compared the performance of the ARCs on the front and back sides of the substrate (Fig. 5). The results showed that the AR layers between the substrate and the ITO layer were more effective in enhancing J_{SC}, particularly when the refractive index is controllable. These findings would be helpful for designing the configuration of ARCs for OPVs.

References

[1] J.C. Wang, W.T. Weng, M.Y. Tsai, M.K. Lee, S.F. Horng, T.P. Perng, C.C. Kei, C.C. Yu, and H.F. Meng, "Highly efficient flexible inverted organic solar cells using atomic layer deposited ZnO as electron selective layer," J. Mater. Chem., vol.20, pp.862–866, 2010.

[2] E. Bundgaard and F.C. Krebs, "Low band gap polymers for organic photovoltaics," Sol. Energ. Mat. Sol. Cells, vol.91, pp.954–985, 2007.

[3] M. Jorgensen, K. Norrman, S.A. Gevorgyan, T. Tromholt, B. Andreasen, and F.C. Krebs, "Stability of polymer solar cells," Adv. Mater., vol.24, pp.580–612, 2012.

[4] J.S. Kim, Y.M. Lee, J.H. Lee, J.H. Park, J.K. Kim, and K. Cho, "High-efficiency organic solar cells based on end-functional-group-modified poly (3-hexylthiophene)," Adv. Mater., vol.22, pp.1355–1360, 2010.

[5] X.Z. Wang, Q.W. Wang, L. Yan, W.Y. Wong, K.Y. Cheung, A.N. Ng, A.B. Djurisic, and W.K. Chan, "Very-low-bandgap metallopolyynes of platinum with a cyclopentadithiophenone ring for organic solar cells absorbing down to the near-infrared spectral region," Macromol. Rapid Commun., vol.31, pp.861–867, 2010.

[6] W. Nie, R. Coffin, J. Liu, C.M. MacNeill, Y. Li, R.E. Noftle, and D.L. Carroll, "Exploring spray-coating techniques for organic cell applications," Int. J. Photoenergy, 175610, 2012.

[7] F.C. Krebs, S.A. Gevorgyan, and J. Alstrup, "A role-to-roll process to flexible polymer solar cells: Model studies, manufacture and operational stability studies," J. Mater. Chem., vol.19, pp.5442–5451, 2009.

[8] M. Niggemann, B. Blasi, A. Gombert, A. Hinsch, H. Hoppe, P.

Lalanne, D. Meissner, and V. Wittwer, "Trapping light in organic plastic solar cells with integrated diffraction gratings," Proc. 17th European Photovoltaic Solar Energy Conference, Munich, Germany, 2001.

[9] M. Niggemann, M. Riede, A. Gombert, and K. Leo, "Light trapping in organic solar cells," Physca Status Solidi a, vol.205, 2862–2874, 2008.

[10] A. Raman, Z. Yu, and S. Fan, "Dielectric nanostructures for broadband light trapping in organic solar cells," Opt. Express, vol.19, pp.19015–19026, 2011.

[11] S.H. Park, A. Roy, S. Beaupr, S. Cho, N. Coates, J.S. Moon, D. Moses, M. Leclerc, K. Lee, and A.J. Heeger, "Bulk heterojunction solar cells with internal quantum efficiency approaching 100%," Nature Photonics, vol.3, pp.297–302, 2009.

[12] W.C. Luk, K.M. Yeung, K.C. Tam, K.L. Ng, K.C. Kwok, C.Y. Kwong, and A.M.C. Ng, "Enhanced conversion efficiency of polymeric photovoltaic cell by nanostructured antireflection coating," Organic Electronics, vol.12, pp.557–561, 2011.

[13] J.Y. Kim, S.H. Kim, H.H. Lee, K. Lee, W. Ma, X. Gong, and A.J. Heeger, "New architecture for high-efficiency polymer photovoltaic cells using solution-based titanium oxide as an optical spacer," Adv. Mater., vol.18, pp.572–576, 2006.

[14] M. Ghebrebrhan, P. Bermel, Y. Avniel, J.D. Joannopoulos, and S.G. Johnson, "Global optimization of silicon photovoltaic cell front coatings," Opt. Express, vol.17, pp.7505–7518, 2009.

[15] Y.J. Chang and Y.T. Chen, "Broadband omnidirectional antireflection coatings for metal-backed solar cells optimized using simulated annealing algorithm incorporated with solar spectrum," Opt. Express, vol.19, pp.A875–A887, 2011.

[16] M.F. Schubert, F.W. Mont, S. Chhajed, D.J. Poxson, J.K. Kim, and E.F. Schubert, "Design of multilayer antireflection coatings made from co-sputtered and low-refractive-index materials by genetic algorithm," Opt. Express, vol.16, pp.5290–5298, 2008.

[17] B. Sopori, J. Amieva, B. Butterfield, and C. Li, "Rapid mapping of AR coating thickness on Si Solar Cells using GT-FabScan 6000," Proc. 31st IEEE Photovoltaics Specialists Conference and Exhibition, Lake Buena Vista, Florida, 2005.

[18] J. Poxson, M.F. Schubert, F.W. Mont, E.F. Schubert, and J.K. Kim, "Broadband omnidirectional antireflection coatings optimized by genetic algorithm," Opt. Letters, vol.34, pp.728–730, 2009.

[19] D. Poitras and J.A. Dobrowolski, "Toward perfect antireflection coatings. 2. Theory," Appl. Opt., vol.43, pp.1286–1295, 2004.

[20] A.H. G.R. Kan and G.T. Timmer, "Stochastic global optimization methods. Part I: Clustering methods," Mathematical Programming, vol.39, pp.27–56, 1987.

[21] J.Q. Xi, M.F. Schubert, J.K. Kim, E.F. Schubert, M. Chen, S.Y. Lin, W. Liu, and J.A. Smart, "Optical thin-film materials with low refractive index for broadband elimination of Fresnel reflection," Nature Photonics, vol.1, pp.176–179, 2007.

[22] H.A. Macleod, Thin-film optical filters, Fourth ed., CRC Press, Boca Raton, 2010.

[23] N.K. Persson and O. Inganas, "Organic tandem solar cells — Modeling and predictions," Sol. Energ. Mat. Sol. Cells, vol.90, pp.3491–3507, 2006.

[24] N.K. Persson and O. Inganas, "Simulations of optical processes in organic photovoltaic devices," pp.107–138. in S.S. Sun and N.S. Sariciftci, eds., "Organic Photovoltaics: Mechanisms, Materials, and Devices," CRC Press, Boca Raton, 2005.

[25] ASTMG173-03, Standard tables for reference solar spectral irradiances, ASTM International, West Conshohocken, Pennsylvania, 2005.

[26] A.Y. Darkwi, W.K. Lote, and K. Ibrahim, "Computer simulation of collection efficiency of a-Si : H tandem solar cells interconnected by transparent conductive oxide," Sol. Energ. Mat. Sol. Cells, vol.60, pp.1–9, 2000.

[27] H. Hoppe, N.S. Sariciftci, and D. Meissner, "Optical constants of conjugated polymer/fullerene based bulk-heterojunction organic solar cells," Mol. Cryst. Liq. Cryst., vol.385, pp.113–119, 2002.

[28] A. Szekeres, T. Ivanova, and K. Gesheva, "Spectroscopic ellipsometry study of CVD molybdenum oxide films: Effect of temperature," J. Solid State Electrochemistry," vol.7, pp.17–20, 2002.

[29] E. Lioudakis, A. Othonos, I. Alexandrou, and Y. Hayashi, "Optical properties of conjugated poly (3-hexylthiophene)/[6,6]-phenylC$_{61}$-butyric acid methyl ester composites," J. Appl. Phys., vol.102, 083104, 2007.

[30] D.E. Gray, American Institute of Physics Handbook, third ed., American Institute of Physics, McGraw-Hill Book Company, New York, 1972.

[31] J.P. Borgono, B. Lazarides, and E. Pelletier, "Automatic determination of the optical constants of inhomogeneous thin films," Appl. Opt., vol.21, pp.4020–4029, 1982.

[32] F. Flory, B. Schmitt, E. Pelletier, and H.A. Macleod, "Interpretation of wide band scans of growing optical thin films in terms of layer microstructure," Proc. Soc. Photo-Opt. Instr. Eng., vol.401, pp.109–116, 1983.

[33] E.D. Palik, Handbook of optical constants of solids, Academic Press, San Diego, 1991.

[34] D. Bouhafs, A. Moussi, A. Chikouche, and J.M. Ruiz, "Design and simulation of antireflection coating systems for optoelectronic devices: Application to silicon solar cells," Sol. Energ. Mat. Sol. Cells, vol.52, pp.79–93, 1998.

[35] S.A. Boden and D.M. Bagnall, "Sunrise to sunset optimization of thin film antireflective coatings for encapsulated, planar silicon solar cells," Prog. Photovoltaics: Res. Appl., vol.17, pp.241–252, 2009.

[36] E. Osorio, R. Urtega, L.N. Acquaroli, G. Garcia-Salgado, H. Juarez, and R.R. Koropecki, "Optimization of porous silicon multilayer as antireflection coatings for solar cells," Sol. Energ. Mat. Sol. Cells, vol.95, pp.3069–3073, 2011.

Shigeru Kubota was born in 1972. He received Ph.D. degree from Tokyo University in 2003. He is now an associate professor in Yamagata University, and is engaged in studies on applied physics and mathematics. His research topic includes the optical analysis of solar cells and the optimization of anti-reflection coatings.

Kensaku Kanomata was born in 1983. He received the B.E. and M.E. degrees in faculty of Engineering from Yamagata University. Currently, he is a candidate for a Ph.D. degree in Graduate school of Science and Engineering in Yamagata University.

Katsuaki Momiyama was born in 1980. He received the B.E. and M.E. degrees in faculty of Engineering from Yamagata University. Currently, he is a candidate for a Ph.D. degree in Graduate school of Science and Engineering in Yamagata University.

Takahiko Suzuki was born in 1966. He finished Graduate School of Textile Science and Technology in Shinshu University in 1991, and received ME degree. He started his engineer's career at TDK Corp. in the same year. He is a technical staff of faculty of Engineering in Yamagata University since 2006, and is engaged in technical support for research and education.

Fumihiko Hirose was born on January 21, 1965. Completed Graduate School of Engineering, Tohoku University in 1992 and received Ph.D. degree there. He is presently a professor in Graduate school of Science and Engineering in Yamagata University. He has been engaged in high quality film deposition techniques, fast switching devices and highly efficient solar cells with interfacial nanotechnologies.